JOURNAL OF THERMOPHYSICS AND HEAT TRANSFER
Vol. 24, No. 3, July–September 2010

Heat Transfer to a Composite Material Under Ice Particle Impacts

Y. K. Hong,* C. Park,† and S. W. Baek‡
Korea Advanced Institute of Science and Technology, Taejon 305-701, Republic of Korea

DOI: 10.2514/1.47776

This paper examines what would happen if a supersonic vehicle flies through an atmosphere laden with ice particles. In previous research of the present authors, an experiment was performed to determine the characteristics of ice-particle impact phenomenon. Therein, the mass loss from the vehicle's surface material by the impacts was measured and the fragments' behavior was studied. In the present work, the trajectories of fragments from the stagnation region were calculated at the experimental conditions. It was surmised that the flow in the stagnation region is turbulent. Turbulent flow increases the heat transfer rate to the surface, and consequently the mass loss increases. To determine the extent of heat transfer rate increase, the new turbulence model, tentatively named crater-induced turbulence model, was proposed. Therein, an assumption was introduced that the turbulent mixing length is proportional to the depth of the impact craters. The constant of proportionality was determined from the existing experimental data taken in wind-tunnel tests. It is shown that heat transfer rate may increase up to 14 times that without ice-particle impacts.

Nomenclature

c_1, c_2, c_3	=	nondimensional coefficient for fragments' mass distribution, Eq. (3)
c_5	=	nondimensional coefficient for fragments' velocity distribution, Eq. (6)
D	=	fragments' diameter
E	=	projectile kinetic energy, J
F	=	distribution function, Eq. (6)
f	=	stream function, Eq. (11).
H	=	flow enthalpy, J/kg
H_v	=	heat of conversion of 1 g of ice at 0°C to steam at 100°C 3012 J/kg
m	=	mass of a particle
q	=	stagnation-point heat transfer rate without ice impact
q_i	=	stagnation-point heat transfer rate with ice impact
q_{st}	=	stagnation-point heat flux
R	=	nose radius
Re	=	Reynolds number
St	=	Stanton number
T	=	temperature, K
t	=	time
u	=	velocity in x direction
V	=	magnitude of velocity, $\sqrt{u^2 + v^2}$
v_i	=	equivalent injection velocity
v	=	velocity in y direction
x	=	horizontal distance
y	=	vertical distance
α_c	=	fraction of ice mass in the atmosphere
β	=	ratio of the target material mass removed by impact to the mass of impacting ice particle
γ	=	nondimensional exponent, Eq. (7)
ΔM	=	displaced mass, g
δ	=	turbulent mixing length
Φ	=	heat flux blockage factor
ϕ	=	inclination angle of the ejecta with respect to the normal
μ	=	viscosity, N-s/m^2
ν	=	turbulent viscosity, N-s/m^2
ρ	=	density
σ	=	scale parameter, Eq. (4)
τ	=	injection-induced turbulence parameter, sec, Eq. (19)
χ	=	fragment mass-to-air mass ratio, $\alpha_c\ (1 + \beta)$
ω	=	half-width angle, deg, Eq. (6)

Subscripts

a	=	ambient condition
D	=	size
i	=	impact
m	=	mass
max	=	maximum value
min	=	minimum value
rel	=	relative value
s	=	shock layer
t	=	target material
v	=	velocity
w	=	wall
ϕ	=	ejecta angle

Presented as Paper 2009-3773 at the 27th AIAA Applied Aerodynamics Conference, San Antonio, TX, 22–25 June 2009; received 22 October 2009; revision received 28 January 2010; accepted for publication 13 February 2010.

*Graduate Student, Department of Aerospace Engineering, Kusung-Dong 373-1, Yusung-Gu. Current address KAPS Company, Number 1512, Dong-a Venture Tower, Bondmyung-dong, Yusung-gu, Daejeon; shinehyk@ymail.com.

†Professor, Department of Aerospace Engineering, Kusung-Dong 373-1, Yusung-Gu. Fellow AIAA.

‡Professor, Department of Aerospace Engineering, Kusung-Dong 373-1, Yusung-Gu. Senior Member AIAA.

I. Introduction

WHEN a high-speed vehicle flies through a cloud of rain drops, snowflakes, or hail, damage may occur to the vehicle. Although hail is rare, rain drops exist as ice particles at high altitudes [1–3]. The impacts of such ice particles on a high-speed vehicle are a concern worthy of study. An environment in which solid or liquid particles impact a flying object is known as an erosive environment. The impacts increase the wearing rate of the surface material by two mechanisms: direct gouging of material by forming impact craters and increase in thermochemical ablation rate by an increase in heat transfer rates. Some amount of research has been carried out on this subject [4,5]. However, the results of such studies have not yet been reported in whole, at least in open literature.

The phenomenon of impact of a solid object with a solid surface at a high speed has been studied and reported in open literature in

connection with the astronomical impacts [6]. It is well known that when an asteroid impacts a planetary surface a crater is formed. In the cratering process the impacting body is fragmented and, when the impact energy is sufficient, it is vaporized. The target surface loses mass by forming a crater. The mass ejected from the surface is also fragmented and sometimes vaporized.

A theoretical model [7] to describe this cratering phenomenon should predict the quantity of the mass removed from the surface and the momentum and energy imparted to the surface. To develop a theoretical model to describe the ice-particle impact phenomenon, the quantity of the mass removed from the surface, the magnitudes of the momentum and energy carried by the issuing mass, and the direction of the issuing mass were measured experimentally [8] by the present authors. The results of this study provide a formula that could be used in determining the surface mass loss rate due to direct gouging.

The behavior of the issuing mass has an impact on the second mechanism of mass removal, i.e., increase in heat transfer rate. It has been observed that, in an erosive environment, the bow shock wave formed over a blunt body bulges forward, and shock layer pressure and heat transfer over the body increase greatly [9,10]. The exact relationship between the mass, momentum, and energy of the issuing mass and the extent of increase in heat transfer is not known presently. However, it is suspected that the increase in the heat transfer is because of the turbulence generated by the fragments [11,12].

The objective of the present work is to study the consequence of ice-particle impacts on heat transfer phenomenon. A composite material is chosen here because it is commonly used as a structural material for high-speed vehicles. A new turbulence model, a modified version of the injection-induced turbulent model [11], is used in describing this heating environment. An assumption was introduced that the turbulent mixing length is proportional to the depth of the impact craters. The constant of proportionality was determined from the existing experimental data taken in wind-tunnel tests. The model is used in determining the heat flux enhancement in the stagnation region.

II. Summary of Earlier Experimental Results

The heatshield of a reentry vehicle is made in many cases with a composite material. One of those composite materials is carbon/epoxy. In [8], the effect of ice-particle impacts on a carbon/epoxy was studied experimentally. An ice projectile was accelerated by a two-stage light gas gun. The Mach number of the projectile ranged from 2 to 3. A carbon/epoxy composite material was prepared for the target specimen. Test sets and results are summarized in Table 1.

In that experiment, a total mass removed from target specimen was determined to be expressible as

$$\Delta M = -0.00327 + 0.000648 \times E \tag{1}$$

In the above equation, ΔM and E denote removed mass in g and projectile kinetic energy in J. From the above equation, crater size was determined as

$$d = \left(\frac{3}{2\pi} \times \frac{\Delta M}{\rho_t}\right)^{1/3} \tag{2}$$

where d is the equivalent crater size.

From here on, attention will be focused on the increase in heat transfer rate due to particle impacts. An impact produces fragments. The issuing fragments consist of the broken-up pieces of the ice projectile and target material in a powered form. The behavior of ice fragments is known from [13]. The behavior of target material was studied using a witness film and a high-speed camera. Figure 1 shows the issuing mass distribution for tests 08071702, 08071703, and 08071802. From Fig. 1, the mass distribution curve was derived as

$$N(>V) = c_1 c_2 \exp\left(-c_2 \frac{V}{V_0}\right) + (1 - c_1) c_3 \exp\left(-c_3 \frac{V}{V_0}\right) \tag{3}$$

where the constants c_1, c_2, and c_3 are 0.2452, 26820, and 4118, respectively. V_0, a scale parameter related to the total volume, is

Table 1 Ice impact test sets for specimens

Test number	Energy, J	Displaced mass, g
08042501	6.812	N/A
08042502	6.516	N/A
08042503	8.224	N/A
08042506	9.593	N/A
08042507	7.647	N/A
08042508	6.107	0.0002
08042601	8.124	0.0018
08042602	8.538	0.0025
08042604	9.988	0.0037
08042605	9.342	0.0026
08042606	6.239	0.0001
08042607	6.812	0.0011
08050901	6.972	0.0014
08050902	6.460	0.0011
09050903	10.313	0.0032
08051001	7.293	0.0016
08051002	6.392	0.0013
08051003	5.428	0.00005
08051101	8.608	0.0024
08051102	6.002	0.00085
08051103	9.778	0.003
08051202	6.820	0.0016
08062701	7.292	0.0010
08062902	5.762	0.0007
08063002	10.598	0.0034
08071702	6.820	N/A
08071703	6.820	N/A
08071802	8.004	N/A

5.332×10^7 μm^3. Scale parameters of ice fragments σ_i and of target σ_t are 52 μm and 35.15 μm, respectively. From these values the representative characteristic length $\sigma$was determined as

$$\sigma = \frac{1}{\left(\frac{V_{\text{ice}}}{V_{\text{ice}}+V_{\text{target}}}\right)^{1/3} + \left(\frac{V_{\text{target}}}{V_{\text{ice}}+V_{t\,\text{arg}\,et}}\right)^{1/3}} \left[\left(\frac{V_{\text{ice}}}{V_{\text{ice}}+V_{\text{target}}}\right)^{1/3} \sigma_t + \left(\frac{V_{\text{target}}}{V_{\text{ice}}+V_{\text{target}}}\right)^{1/3} \sigma_i\right] \tag{4}$$

where V_{ice} and V_{target} are volumes of fragments of ice projectile and target material, respectively.

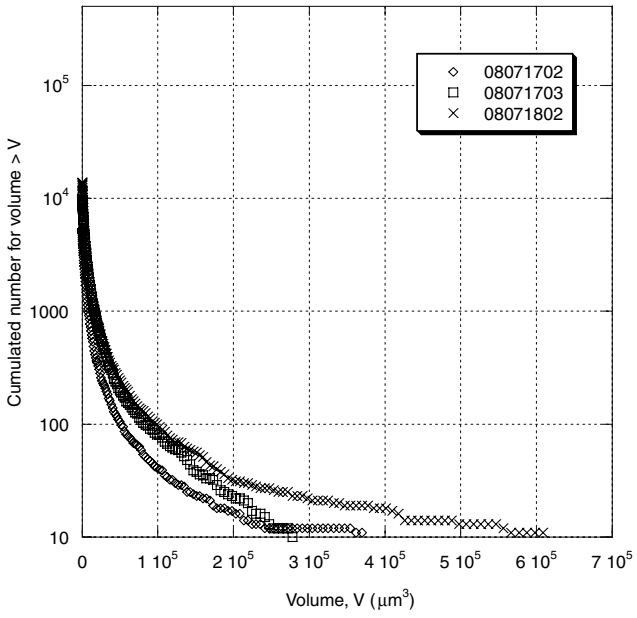

Fig. 1 Cumulated number larger than volume (V) for tests 08071702, 08071703, and 08071802.

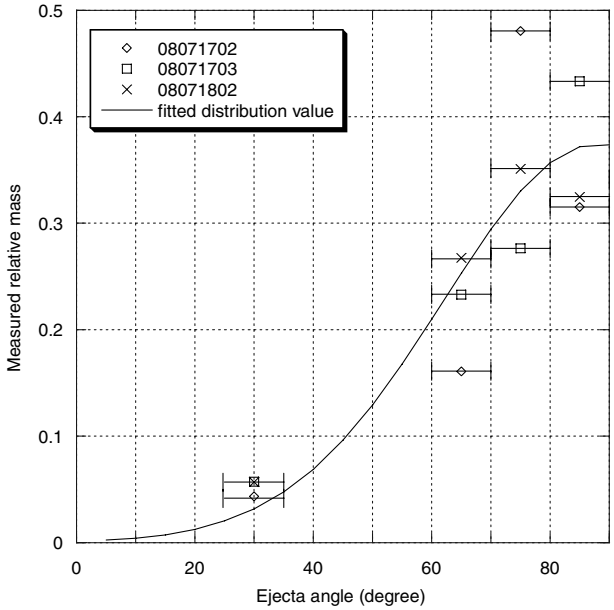

Fig. 2 Relationship between ejected mass and ejecta angle for tests 08071702, 08071703, and 08071802. The open symbols mean the experimental data, and the horizontal bar indicates the measured angle intervals.

The directional distribution of solid particles is shown in Fig. 2. Ejecta angle ϕ is the direction of ejecta fragments, i.e., inclination angle with respect to the normal direction. From this figure, it can be found that many solid particles are issued at high angles.

The fragments' velocity was also empirically formulated in [8] as

$$V(D,\phi) = V_i \cdot F_{v,\phi}(\phi) \cdot F_{v,D}(D) \tag{5}$$

where V is the fragments' velocity and V_i is the projectile velocity. Here, $F_{v,\phi}(\phi)$ represents the effect of ejecta angle. Figure 3 shows the fragments' velocity divided by the projectile velocity in the ejecta angle region for several tests. The line fitted to the data is

$$F_{v,\phi}(\phi) = c_5 \exp\left(\left(-\frac{(\phi-\phi_{v,\max})^2}{2\omega_v^2}\right)\right) \tag{6}$$

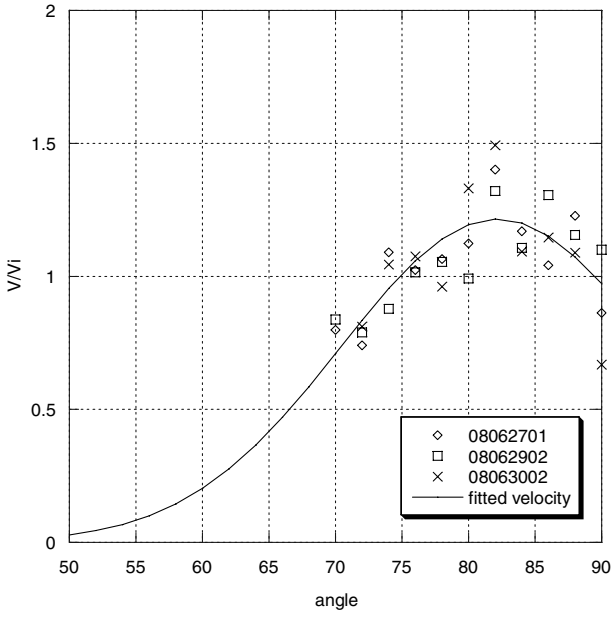

Fig. 3 Relationship between $V_{\max}(\theta)/V_i$ and ejecta angle. The open symbols represent the experimental data and the solid line is a Gaussian profile fit to the data.

where constant c_5 is 1.2152, and $\phi_{v,\max}$, the angle where the maximum fragment velocity occurs, and ω_v, the half-width, are 82.12 and 11.706 deg, respectively.

In Eq. (5), $F_{v,D}(D)$ represents the effect of fragments' size D

$$F_{v,D}(D) = \left(\frac{D}{D_{\min}}\right)^{-\gamma} \tag{7}$$

where $D_{\min}$ and exponent γ are 1 μm and 0.366, respectively.

III. Motion of Rebounding Fragments

A. Governing Equations

Motion of solid particles issuing from the heat shield wall was studied in [14–16]. In those studies, the issuing particles were assumed to be spherical in shape, and so the drag coefficient would be unity, which is the Newtonian value. This assumption was made here also. The density of the fragments was assumed to be that of ice, that is 0.919 g/cm^3.

To simplify the problem, only the stagnation region flow, sketched in Fig. 4, was considered here. The motion of an issuing fragment was dictated by the Newton's equation of motion. The force acting on a particle is the drag. It was calculated as a vectorial sum of the force due to flow motion and force due to particle motion. The angle between the flow and the particle is described by θ. The x- and y-components of the drag force produce the acceleration

$$m\frac{\mathrm{d}u}{\mathrm{d}t} = -\text{drag} \times \cos(\theta) \qquad m\frac{\mathrm{d}v}{\mathrm{d}t} = -\text{drag} \times \sin(\theta) \tag{8}$$

The particle is heated on the windward side. Total heat transfer to the particle is calculated as the product of the stagnation-point heat transfer rate and the frontal surface area $\pi(D/2)^2$. In the calculation of the stagnation-point heat transfer rate, a simplification $\rho\mu=$ constant, is made. Using Goulard's analysis and approximating the parameter $\sqrt{\rho_a/\rho_s}$ to be $\sqrt{1/8}$, the Goulard's formula [17] for stagnation-point heat transfer rate q_{st} becomes

$$q_{\mathrm{st}} = 0.590\rho V_{\mathrm{rel}}(H - H_w)/\sqrt{Re} \tag{9}$$

where the density ρ is ρ_s when the particle is inside the shock layer and ρ_a when it is outside of the shock layer. The Reynolds number Re is

$$Re = \frac{\rho V_{\mathrm{rel}}(D/2)}{\mu_a} \tag{10}$$

The flow and wall enthalpy difference $H - H_w$ is $V_{\mathrm{rel}}^2/2 + 1006 \times (T - T_w)$ in J/kg.

Because of vaporization, the heat transfer rate is convectively blocked partly. By defining the stream function f by

$$f = -\frac{\rho v}{\sqrt{2\rho_s\mu_s(\mathrm{d}u/\mathrm{d}x)}} \tag{11}$$

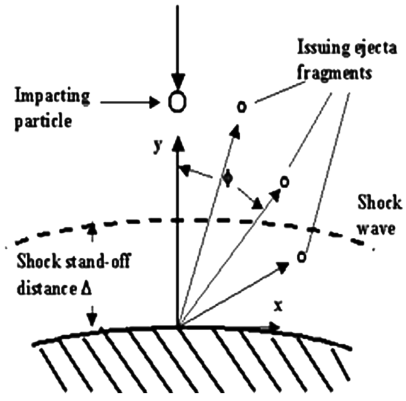

Fig. 4 Schematic of the flowfield of ice-impact phenomenon.

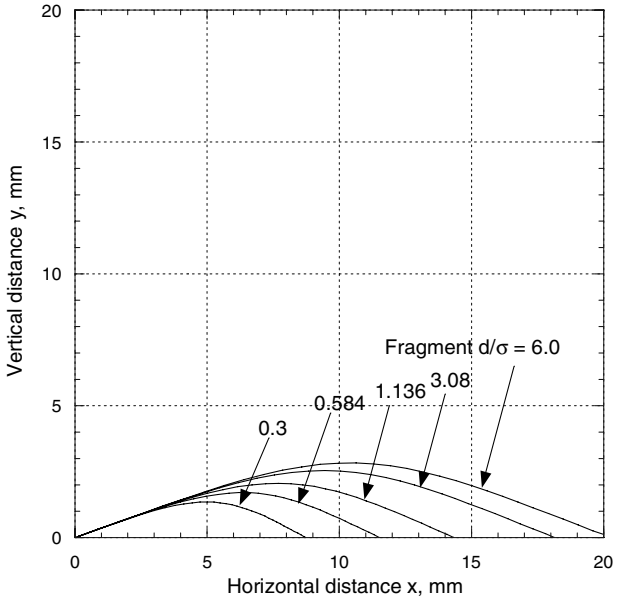

Fig. 5 Trajectories of rebounding fragments issuing at $\phi = 70$ deg.

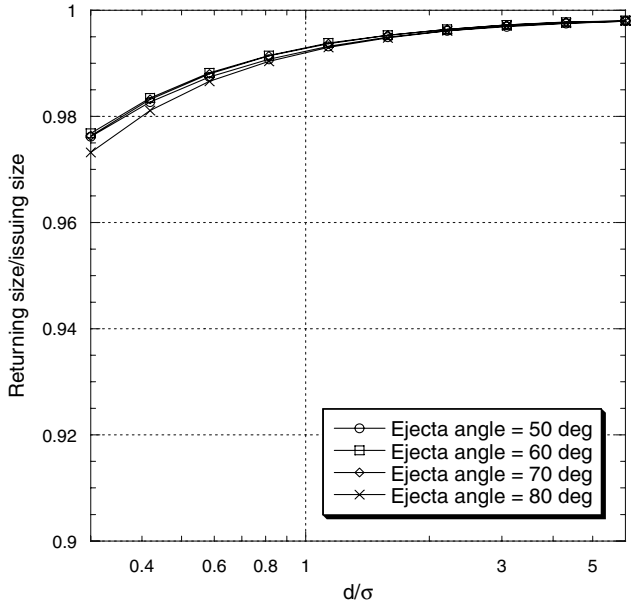

Fig. 6 Size ratio between issuing particles and return-hit particles.

the heat transfer rate to a vaporizing surface is the value given by Eq. (9) times the blockage factor Φ, which is smaller than one and is a function of the wall value of f. The acceleration parameter $\mathrm{d}u/\mathrm{d}x$ is given from the Newtonian theory as

$$\frac{\mathrm{d}u}{\mathrm{d}x} = \frac{V_{\mathrm{rel}}}{D/2}\sqrt{2\rho_a/\rho_s} \tag{12}$$

Numerical solution of the heat transfer problem, such as that in [16], shows that Φ is approximately a linear function of f_w in the small range of f_w, as

$$\Phi = 1 - f_w \tag{13}$$

The mass flow rate of the vapor at the stagnation point of a fragment ρv, appearing in Eq. (11), is calculated in general by dividing the heat transfer rate value q_{st} by the heat of vaporization $H_v = 3012$ J/kg

$$\Phi = 1 - \frac{q_{\mathrm{st}}/H_v}{\sqrt{2\rho_s\mu_s(\mathrm{d}u/\mathrm{d}x)_w}} \tag{14}$$

Therefore, the blockage-corrected stagnation-point heat transfer rate q_{st} satisfies the equation

$$q_{\mathrm{st}} = \frac{0.590\rho V_{\mathrm{rel}}(H - H_w)}{\sqrt{Re}}\left(1 - \frac{q_{\mathrm{st}}/H_v}{\sqrt{2\rho_s\mu_s(\mathrm{d}u/\mathrm{d}x)}}\right) \tag{15}$$

By solving the above equation for q_{st}, one obtains

$$q_{\mathrm{st}} = \frac{0.590\rho V_{\mathrm{rel}}(H - H_w)/\sqrt{Re}}{1 + 0.590(h - h_w)/H_v} \tag{16}$$

By dividing this q_{st} by H_v, one obtains the rate of vaporization of the fragment. Thus, the equation governing the mass of the fragment is

$$\frac{\mathrm{d}m}{\mathrm{d}t} = -\frac{q_{\mathrm{st}}}{H_v} \times \pi(D/2)^2 \tag{17}$$

B. Calculated Fragments' Behavior in Shock Layer

In Fig. 5, the trajectories of the rebounding fragments are shown for those issuing from the ejecta angle ϕ of 70 deg for the experimental condition, i.e., mass of ice particle $=0.01884$ g and impact velocity $=1000$ m/s, at 5 km altitude. This is the third representative flight condition listed in Table 2. The issuing velocity of each fragment is given by Eq. (5). Sizes of the fragments ranging from $D/\sigma = 0.3$ to 6.0 are shown. One notices in this figure that all particles turn back and reach the wall.

Figure 6 shows the mass variation in the shock layer in detail. As mentioned in the previous section, the most fragments are issuing at high ejecta angles ($50 \sim 80$ deg). Therefore, only the higher ejecta angle fragments are considered. The returning size of a fragment is larger than 96% of the initial size of that fragment. From this figure, it can be said that most fragments survive in the shock layer.

The trajectories of $D/\sigma = 1.136$ are shown for different ejecta angles in Fig. 7. As mentioned before, this figure also considered the only high ejecta angle fragments.

From [10–12], it is known that an erosive environment makes flow turbulent in the stagnation region. From the above results, it can be said that the ice-particle impact can also make flow turbulent because all fragments still exist in the stagnation region even though they are partly vaporized. It means that the removed mass determined from the experimental results can be used as the mass injection rate in

Table 2 Selected flow environment and stagnation-point heat flux rate enhancement factor calculated by crater-induced turbulence model[a]

Altitude, km	Density, kg/m^3	Flight velocity, m/s	Ice projectile mass, mg	β	σ, μm	q_i/q
5.0	0.746	500	18.84	0	52	1
10.0	0.403	500	18.84	0	52	1
5.0	0.746	1000	18.84	0.1504	45.9	6.24
10.0	0.403	1000	18.84	0.1504	45.9	4.62
5.0	0.746	1500	18.84	0.555	43.9	9.38
10.0	0.403	1500	18.84	0.555	43.9	6.91
5.0	0.746	2000	18.84	1.122	42.8	13.67
10.0	0.403	2000	18.84	1.122	42.8	10.06

[a]Ice mass fraction α_c is 0.002.

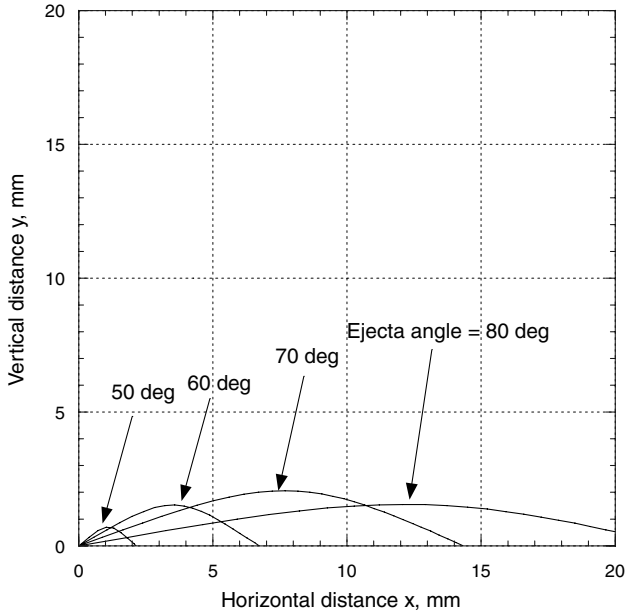

Fig. 7 Trajectories of rebounding fragments issuing ($d/\sigma = 1.136$) at various ejecta angles.

implementing the turbulence model in the following section. The impacts at the stagnation point produce ejecta that travel downstream because their path angles are large. But at the same time, the impacts at a downstream point send a portion of their ejecta upstream toward and beyond the stagnation point.

IV. Application of Turbulence Model

In [12], Hove and Shih recognized that the kinetic energy of the ice particles in the freestream is equivalent to turbulence energy in the shock layer. The presence of ice particles in the freestream is thus equivalent to having a turbulent freestream flow. Hove and Shih [12] point out that such an increase in the effective turbulence level cannot increase the heat transfer rate in the stagnation region; the flow in the stagnation region moves so slowly that the boundary layer tends to become laminar even when the freestream flow is turbulent. The explanation of the enhanced heat transfer rate offered by Hove and Shih was that the surface roughness caused by the ice-particle impacts produced the enhancement. Rough surfaces are known to increase the wall heat transfer rate greatly in most cases. However, this explanation is invalid in the stagnation region; it is known that the stagnation-point flow is always laminar even when the surface is rough, provided there is no mass flow injection from the wall [11].

However, there is a valid explanation of the heat transfer rate enhancement that has never been invoked before. The issuing of fragments from the wall after impact is a form of mass injection from the wall. In [11], Park theorized that an injection from the stagnation-point wall induces turbulence and makes the boundary layer turbulent there. Several experimental evidences are given in that work to show that the boundary-layer flow is indeed turbulent in the presence of wall injection.

A. Description of Existing Injection-Induced Turbulence Model

According to Park's theory [11], the turbulent viscosity at wall ν_w is expressed as

$$\nu_w = 0.4\dot{m}\delta \tag{18}$$

where $\dot{m}$ is the mass flow rate of injection $\dot{m} = \chi\rho_a V_a$. The mixing length δ is given by

$$\delta = \delta_{\max}[1 - \exp(-\tau v_i/\delta_{\max})] \tag{19}$$

where

$$\delta_{\max} = \max\left[35\sqrt{\frac{\rho_s\mu_s}{2(\mathrm{d}u/\mathrm{d}s)}}, 0.1(p/250)^{1/2}\right] \tag{20}$$

and

$$\frac{\mathrm{d}u}{\mathrm{d}s} = \frac{V_a}{R}\sqrt{\frac{2\rho_a}{\rho_s}} \tag{21}$$

Here, v_i is the equivalent injection velocity, which, in the present case, becomes

$$v_i = \chi\rho_a V_a/\rho_s \tag{22}$$

The time parameter τ was determined empirically to fit the existing ablation data.

In a flow not containing particles, this turbulence energy at the wall decays in the boundary layer by the natural decay process such as that described by the k-ε model [11]. However, in the present case of ice-particle impact, all fragments remain in the boundary layer. Therefore, the turbulent intensity created at the wall ν_w will not decay. Thus, the wall heat transfer rate in this case can be calculated by replacing the viscosity μ in the well-known heat transfer rate equation by the effective (combined) viscosity $\mu + \nu_w$. Because heat transfer rate is proportional to the square root of viscosity, the enhancement ratio q_i/q is simply

$$\frac{q_i}{q} = \sqrt{\frac{\mu + \nu_w}{\mu}} \tag{23}$$

This relationship holds even when the heat transfer occurs mostly in the form of surface recombination, because the coefficients of effective species diffusion are proportional to the effective viscosity.

B. New Turbulent Model for Impacting Environment

An improvement to the theory in [11] is proposed in the present work by using the fact that an ice-particle impact produces a crater. This method is tentatively named the crater-induced turbulence (CIT) model. In flight, even though ice-particle impacts occur at finite intervals, the phenomenon is cumulative. As a result, the heatshield surface will be mostly covered by impact craters. Each crater will produce a local vortex flow motion as shown in Fig. 8. Therefore, it would seem more appropriate to relate the turbulence mixing length to the dimensions of the crater. It is proposed that the mixing length in Eq. (20) is expressible as

$$\delta_m = \alpha \times \text{crater depth} \tag{24}$$

where the crater depth is given by Eq. (2).

The CIT model still uses the time constant τ in Eq. (19). The constant of proportionality α and the time constant τ are determined by comparing with the experimental data of Dunbar obtained in a wind tunnel, as given below.

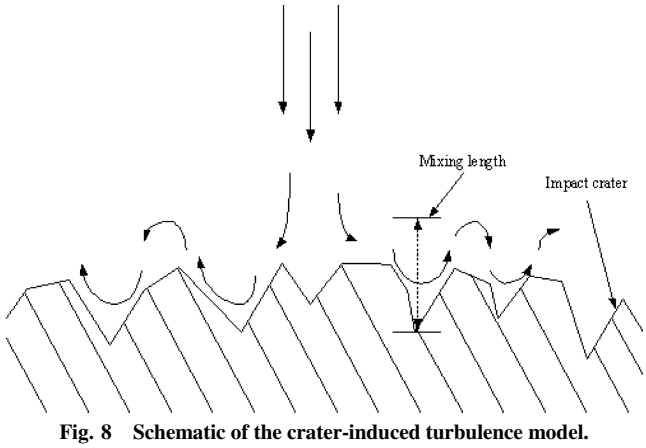

Fig. 8 Schematic of the crater-induced turbulence model.

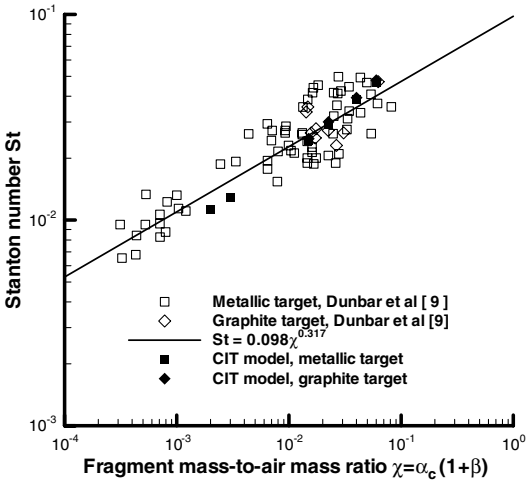

Fig. 9 Comparison of Stanton number between the injection-induced turbulence model and wind-tunnel data for the representative wind-tunnel conditions $\rho_a = 0.0537$ kg/m^3 and $U_a = 1100$ m/sec using $\alpha = 5.0$ and $\tau = 5 \times 10^{-3}$.

C. Application of the Crater-Induced Turbulence Model to Dunbar et al.'s Results

In [9], Dunbar et al. measured heat flux increase by particle impacts in a wind tunnel. Solid particles (magnesium oxide, silicone carbide, and glass particles) impacted the graphite and metallic materials, such as titanium, inconel, stainless steel, and platinum in their experiment. They plotted the stagnation-point heat transfer rate values obtained using the Stanton number St

$$St = \frac{\text{Heat transfer rate}}{\rho_a U_a (H_a - H_w)} \tag{25}$$

This result is reproduced in Fig. 9. Here, the abscissa $\chi = \alpha_c(1 + \beta)$ is the ratio of the mass flux of fragments rebounding from the target wall to the air mass flux. The fragments consist of the projectile particles and the target material. As seen in the figure, the heat transfer rate increases by several factors due to the particle impacts in the tested range of conditions.

The data in Fig. 9 cover the stagnation-point pressure values from about 0.2 to about 2 atm, and enthalpy values from about 0.28 to 4.2 MJ/kg. The freestream velocities are in the range from 760 to 1700 m/s, and the freestream densities are in the range from 0.0312 to 0.0692 kg/m^3. These values are used in calculating the heat flux enhancement using the CIT model. In [9], Dunbar et al. fitted the wind-tunnel data by an expression

$$St = 0.098\chi^{0.317} \tag{26}$$

This relation between the particle loading and heat transfer rate deduced by Dunbar et al. is used in the present work.

In [18,19], an impact experiment was conducted against metallic targets and graphite targets. The relationship between the depths of the created craters, impact velocity, and projectile diameter observed in their experiment is fitted in the present work by

$$\delta_m = \alpha \times (-0.835 + 0.00251 \times V_i) \times \text{projectile diameter}$$

for metallic target

$$\delta_m = \alpha \times (1.073 + 0.00226 \times V_i) \times \text{projectile diameter}$$

for graphite target (27)

Because Dunbar et al.'s experiment used metallic and graphite targets, these crater depth values are substituted in Eq. (19) to determine the mixing length for Dunbar et al.'s [9] test conditions. In doing so, it became necessary to know the value of χ in the absence of impacts. The lowest value in Dunbar et al.'s experimental data $\chi = 4 \times 10^{-4}$ was considered to be the condition of no ice-particle impacts.

The α and τ values can both be determined by demanding that Dunbar et al.'s experimental data are reproduced at more than one data points. The α and τ values so determined are used in calculating the heat transfer rate to the stagnation point in the presence of ice-particle impacts. By dividing this heat transfer rate by that without ice-particle impacts, the enhance ratio q_i/q [see Eq. (23)] is determined.

The enhancement factor is calculated for the representative wind-tunnel test case $\rho_a = 0.0537$ kg/m^3 and $U_a = 1100$ m/sec using $\alpha = 5.0$ and $\tau = 5 \times 10^{-3}$. The results are presented in Fig. 9.

In Fig. 10, calculation is made for the 1100 m/s case with ρ_a values of 0.0313, 0.0537, and 0.0692 kg/m^3. As seen in Fig. 10, there is a fair agreement between the present calculation and the wind-tunnel data.

D. Application of the Crater-Induced Turbulence Model to the Experimental Condition

The above procedure leads to the expression for the heat transfer rate in the presence of ice-particle impacts

$$\frac{q_i}{q} = \sqrt{\frac{\mu + \nu_w}{\mu}} \tag{28}$$

where ν_w is the turbulent viscosity at the wall given by Eq. (18), $\nu_w = 0.4\dot{m}\delta$. Here, $\dot{m}$ is the mass flow rate of injection $\dot{m} = \chi\rho_a V_a$. This mass flow rate is determined using the experimental results obtained by present authors and calculation results of Sec. III. The mixing length δ is given by Eq. (19), $\delta = \delta_{\max}[1 - \exp(-\tau v_i/\delta_{\max})]$. The maximum mixing length $\delta_{\max}$ is

$$\delta_{\max} = \alpha \times \left(\frac{3}{2\pi} \times \frac{\Delta M}{\rho_t}\right)^{1/3} \tag{29}$$

This maximum mixing length $\delta_{\max}$ is determined using the experimental results obtained by the present authors, Eq. (2).

Using the α value of 5.0 and the τ value of 5×10^{-3} sec, which are determined from Dunbar's study as explained in the previous chapter, the heat transfer rate enhancement factor was calculated. In doing so, ice mass fraction α_c is assumed as 0.002. This mass fraction is deduced from the flight measurement in [1–3], and is the average mass fraction of ice in the atmosphere. The β values are calculated by using the experimental results obtained by the present authors, Eq. (1), and σ values are calculated by Eq. (4).

The results are presented in Table 2 and Fig. 11 for several representative flight conditions. As can be seen in the table and the figure, there is no heat transfer enhancement when the flight velocity is 500 m/s. This is because craters are not formed at the vehicle's surface. But when the flight velocity is greater than 1000 m/s, the

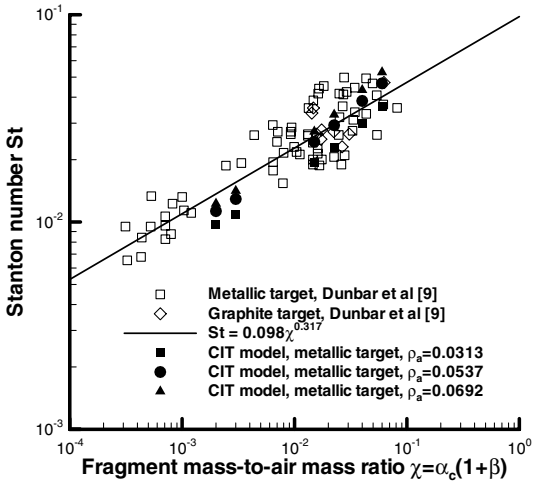

Fig. 10 Comparison of Stanton number between the crater-induced turbulence model and wind-tunnel data for $U_a = 1100$ m/sec and three ρ_a values.

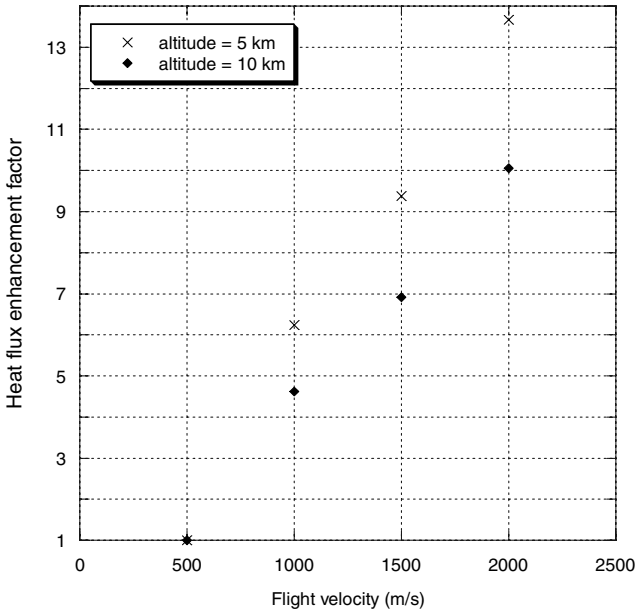

Fig. 11 Stagnation-point heat flux rate enhancement factor calculated by crater-induced turbulence model. Ice mass fraction α_c is 0.002.

heat transfer rates are higher. At the altitude of 5 and 10 km, the enhancement factor becomes up to about 10 and 14, respectively.

V. Conclusions

In the present work, the authors' earlier experimental work is summarized first. From those results, trajectories of fragments were calculated. Fragments are only slightly vaporized and stay as solid particles in the stagnation region. These fragments can produce a turbulent flow in the stagnation region. When the flow becomes turbulent, the heat transfer rate increases. The enhancement of heat transfer rate is determined by a new model tentatively named the CIT model. In this model, an assumption was made that the turbulent mixing length in the model is proportional to the depth of the impact craters. The constant of proportionality was determined from the existing experimental data taken in wind-tunnel tests. The model is used in determining the heat flux enhancement in the stagnation region. Sample calculations of the heat transfer rate enhancement factor so derived were made for several representative flight conditions of high-speed vehicles. It is shown that the heat transfer rate may increase up to 14 times that without ice-particle impacts in an icing environment.

Acknowledgments

This work is the outcome of the Manpower Development Program for Energy and Resources supported by the Ministry of Knowledge and Economy. The authors also thank Kwang June Kim and Ki Sun Kim of the Mechanical Engineering Department of the Korea Advanced Institute of Science and Technology for valuable assistance and discussions.

References

[1] Jeck, R., "A New Database of Snow and Ice Particle Measurements at Altitudes up to 30,000 Ft (9 km)," AIAA Paper 90-0195, Jan. 1990.

[2] Patnoe, M. W., and Moravec, B. A., "Rain and Hail Threat to Aviation: A Probability Analysis of Extreme Rain/Hail Concentrations Aloft," AIAA Paper 97-5654, Oct. 1997.

[3] Moravec, B. A., and Patnoe, M. W., "Recommended Values of Rain and Hail Concentrations to be Considered in the Design of Turbine Engines," AIAA Paper 97-5655, Oct. 1997.

[4] Fleener, W. A., and Watson, R. H., "Convective Heating in Dust-Laden Hypersonic," AIAA Paper 73-761, July 1973.

[5] Shic W. C. L., "Ballistic Range Measurement of Aerodynamic Heating in Erosive Environments," AIAA Paper 76-319, July 1976.

[6] Melosh, H. J., "Cratering Mechanics: Contact and Compression Stage," *Impact Cratering*, Oxford Univ. Press, New York, 1989, pp. 46–60.

[7] Gault, D. E., and Heitowit, E. D., "The Partition of Energy for Hypervelocity Impact Craters Formed in Rock," NASA TM-X-57428, Jan. 1963.

[8] Hong, Y. K., Park, C., and Baek, S. W., "High Velocity Impact of Ice Particles on a Composite Material," *Journal of Composite Materials*, Vol. 43, No. 17, 2009, pp. 1819–1834. doi:10.1177/0021998309340059

[9] Dunbar, L. E., Courtney J. F., and McMillen, L. D., "Heating Augmentation in Erosive Hypersonic Environments," *AIAA Journal*, Vol. 13, No. 7, 1975, pp. 908–912. doi:10.2514/3.60468

[10] Holden, M. S., Gustafson, G. Q., Duryea, G. R., and Hudack L. T., "An Experimental Study of Particle-Induced Convective Heating Augmentation," AIAA Paper 76-320, July 1976.

[11] Park, C., "Injection-Induced Turbulence in Stagnation-Point Boundary Layers," *AIAA Journal*, Vol. 22, No. 2, 1984, pp. 219–225. doi:10.2514/3.8371

[12] Hove, D. T., and Shih, W. C., "Re-Entry Vehicle Stagnation Region Heat Transfer in Particle Environments," *AIAA Journal*, Vol. 15, No. 7, 1977, pp. 1002–1005. doi:10.2514/3.60741

[13] Kato, M., Iijima, Y., Arakawa, M., Okimura, Y., Fujimura, A., Maeno, N., and Mizutani, H., "Ice-on-Ice Impact Experiments," *Icarus*, Vol. 113, No. 2, 1995, pp. 423–441. doi:10.1006/icar.1995.1032

[14] Davies, C. B., and Park, C., "Trajectories of Solid Particles Spalled from a Carbonaceous Heat Shield," *Entry Vehicle Heating and Thermal Protection Systems: Space Shuttle, Solar Starprobe, Jupiter Galileo Probe, Progress in Astronautics and Aeronautics*, edited by P. Bauer and H. Collicott, Vol. 85, AIAA, New York, 1983, pp. 472–495.

[15] Park, C., "Interaction of Spalled Particles with Shock Layer Flow," *Journal of Thermophysics and Heat Transfer*, Vol. 13, No. 4, 1999, pp. 441–449. doi:10.2514/2.6482

[16] Park, C., Raiche G. A., II, and Dirver, D. M., "Radiation of Spalled Particles in Shock Layers," AIAA Paper 2004-1349, 2004.

[17] Goulard, R., "On Catalytic Recombination Rates in Hypersonic Stagnation Heat Transfer," *Jet Propulsion*, Vol. 28, No. 11, 1958, pp. 737–746.

[18] Yoshinori, I. O., Kazuo, N., Yukimasa, I., Yasuo, K., and Toshinori, T., "Damage Behavior of Metallic Materials Caused by Subsonic to Hypervelocity Particle Impact," *Wear*, Vol. 258, 2005, pp. 100–106. doi:10.1016/j.wear.2004.04.013

[19] Yasuhiro, T., Tohru, S., Takashi, A., and Akira, S., "Crater Formation of Carbon Materials by Impact of a High Velocity Sphere," *Carbon*, Vol. 33, No. 11, 1995, pp. 1547–1552. doi:10.1016/0008-6223(95)00113-R